Contribution from the Laboratory for Physical Chemistry, Swiss Federal Institute of Technology, ETH-Zentrum, CH-8092 Zürich, Switzerland, and Swiss Federal Institute for Water Resources and Water Pollution Control (EAWAG), CH-8600 Dübendorf, Switzerland

Modes of Phosphate Binding to Copper(II): Investigations of the Electron Spin Echo Envelope Modulation of Complexes on Surfaces and in Solutions

Wolfgang Möhl,[†] Arthur Schweiger,*[,†] and Herbert Motschi[‡]

Received November 21, 1988

Transition-metal binding (e.g. Cu(II)) to hydrous oxide surfaces (e.g. δ-Al_2O_3) is investigated in the presence of different classes of phosphates. The interactions between the Cu(II) ion and orthophosphate, pyrophosphate, tripolyphosphate, nitrilotris(methylene)triphosphonate (NTP), and glucose phosphate are studied in aqueous solutions in the presence and absence of δ-Al_2O_3 by applying ESR techniques (ENDOR and ESEEM). While ESR parameters are not subject to significant changes due to ligand exchange reactions, ESEEM analyses show distinct patterns by ^1H, ^{31}P, and ^{27}Al modulations, which are complemented by the ENDOR spectrum of the ternary surface complex in the case of CuNTP adsorbed onto δ-Al_2O_3. Chelate-forming classes of phosphate coordinate by an inner-sphere type of bonding to the Cu(II) ion in aqueous solutions whereas glucose phosphate binds through an ion association mechanism (i.e. outer-sphere) and orthophosphate precipitates as an insoluble salt. The affinity of most phosphates for hydrous aluminum oxide does prevail over copper complex formation to such an extent that ternary surface complexes of the type ≡AlO(CuL) disproportionate into ≡Al(L) + ≡AlO-Cu except for L = NTP.

I. Introduction

Chemical compositions of natural water systems and of soil constituents are largely influenced by the interactions taking place at the solid/solution interface. This is reflected in a growing interest to combine interdisciplinary efforts to acquire a more profound understanding of the fundamental processes in the surface chemistry of hydrous oxides and biological debris. Retention and release of heavy metals and of nutritional material is mediated by surface chemical processes as well as dissolution rates of mineral oxides and the nucleation of a new solid phase.

Controversial models[1] have arisen concerning the nature of the chemical or physical bond of the formed surface complex. Adsorption isotherms can be simulated by introducing surface electrochemical equilibrium parameters, e.g. of the form of the Gouy-Chapman-Stern theory, both for metal cations and ligand anions.[2] Attempts to separate Coulomb interactions from chemical components of the total adsorption energy cannot be achieved because the individual thermodynamic parameters are not accessible experimentally. Therefore, drawing conclusions about the physicochemical nature of metal/ligand interactions with surface functional groups of hydrous oxides from thermodynamic measurements is inappropriate. Distinguishing ion association (electrostatic or outer-sphere bonding) from chemical bond formation (inner-sphere bonding or surface complex formation) can be achieved, at least in a qualitative manner, by applying magnetic resonance techniques.

Discrete site chemisorption of transition-metal ions (Cu(II), $V^{IV}O$) has been identified on the surface of hydrous aluminum oxide (δ-Al_2O_3)[3] and on the bacterium *Klebsiella pneumoniae*[4] by applying magnetic resonance techniques such as ESR (electron spin resonance), ENDOR (electron nuclear double resonance), and ESEEM (electron spin echo envelope modulation). Mutual enhancement of the adsorption of metal ions in the presence of organic ligands and vice versa has been attributed to ternary surface complex formation.[5] Interactions of inorganic anions (sulfate, carbonate, phosphate) with surface functional groups in the presence of transition-metal ions have been poorly investigated mainly due to the lack of sensitive methods. The reactivity and residence time of these ionic water constituents, however, is largely influenced by their chemical occurrence, i.e. whether they are chemisorbed, incorporated in a surface precipitate, or retained by ion association.

Among these ions, the phosphorus-containing molecules have received special attention because of their coupling with life cycles and the nutritional limiting factor this element plays in many natural waters.[6] Little is known about its transition between the "burial" state in rocks or sediments and the incorporation into biological systems, except that it goes through stages of adsorption.

In order to achieve a better understanding of these sorption processes, we have investigated for a number of phosphate ligands their interactions with Cu(II) as a representative transition-metal ion in the presence and absence of hydrous δ-Al_2O_3 (as a model clay fraction). In the following, we present the results of a broad systematic ESR and ESEEM study with a class of phosphates covering inorganic and organic forms as well as monodentate and chelating ligands, ortho-, pyro-, and tripolyphosphate, glucose phosphate, and nitrilotris(methylene)triphosphonate (NTP).

II. Experimental Section

(A) Sample Preparation. The Cu^{II}(aquo) complex (5×10^{-3} M) was prepared with $Cu(NO_3)_2 \cdot 6H_2O$. $Cu^{II}L_n$ complexes were prepared by adding 10 mL of a 0.75×10^{-2} M aqueous solution of $Cu(NO_3)_2 \cdot 6H_2O$ to a 10-mL aqueous solution of the ligand L in the ratios $[L]_{tot}/[Cu]_{tot} = n$ with L = glucose phosphate (n = 1), orthophosphate (n = 1), pyrophosphate, (n = 1,2), tripolyphosphate (n = 1, 2), and NTP (n = 1). The pH was raised to 7.5 with KOH, and 5 mL of H_2O was added. If L was only commercially available as a sodium salt, sodium was replaced by potassium to avoid confusions between Na and Al oscillations (ratio of Larmor frequencies of Na and Al: $\nu_{Na}/\nu_{Al} = 1.015$) in the ESEEM patterns. An equal volume of glycerol was added to the solutions to promote glass formation on freezing.

For the preparation of the surface complexes "Aluminoxid C" (Degussa, Frankfurt, West Germany) with a surface area of 100 m^2/g was used without further purification. Adsorption was achieved by first suspending 1 g of δ-Al_2O_3 in 10 mL of doubly distilled water to which KNO_3 and $Cu(NO_3)_2 \cdot 6H_2O$ were added to give a final concentration of 0.1 M (=constant ionic strength) and 10^{-3} M, respectively, for a total volume of 25 mL. The pH was adjusted with 0.1 M KOH (and 0.1 M HNO_3) within 30 min to pH 8.6. After 24 h the suspension was centrifuged and separated from the supernatant solution. The resulting gel was dried at room temperature.

Surface complexes of Cu^{2+}(aq) on δ-Al_2O_3 were prepared by adding the ligands L in the ratios $[L]_{tot}/[Cu^{2+}]_{tot} = 2$ and $[Cu^{2+}]_{tot}/[\equiv AlOH]_{tot} = {}^1/_8$, i.e. 12.5% of the exchange capacity of the surface functional groups of δ-Al_2O_3.

(B) Equipment. Three spectrometers were employed. The ESR spectra were recorded at 90 K on an ESP 300 system from Bruker Physics operating at X-band frequency. The continuous-wave ENDOR spectrometer is based on a Varian E-line with an ENDOR accessory of our own design.[7] Double coding was used (magnetic field modulation 35 Hz; modulation of the radio frequency field 4 kHz). Pulsed ESR measurements were carried out on a homebuilt spectrometer[8] equipped

[†] Swiss Federal Institute of Technology.
[‡] Swiss Federal Institute for Water Resources and Water Pollution Control.

(1) Westall, J. C.; Hohl, H. *Adv. Colloid Interface Sci.* **1980**, *12*, 265.
(2) Westall, J. C. In *Aquatic Surface Chemistry*; Stumm, W., Ed.; John Wiley: New York, 1987; p 3.
(3) Motschi, H.; Rudin, M. *Colloid Polymer Sci.* **1984**, *262*, 579.
(4) Möhl, W.; Motschi, H.; Schweiger, A. *Langmuir* **1988**, *4*, 580.
(5) Rudin, M.; Motschi, H. *J. Colloid Interface Sci.* **1984**, *98*, 385.
(6) Schindler, P. W. *Science* **1974**, *184*, 897.
(7) Forrer, J.; Schweiger, A.; Günthard, Hs. H. *J. Phys. E* **1977**, *10*, 470.

0020-1669/90/1329-1536$02.50/0

with a fast pulse sequence generator (1-ns resolution) and a bridged loop-gap resonator.[9] In all ESEEM experiments, the two-pulse sequence with pulse length of 10–20 ns was used. The time was increased in increments of $\Delta\tau$ = 10 ns. The pulse repetition rate was 1 kHz. ENDOR and ESEEM signals were recorded at temperatures between 8 and 20 K with a helium gas cooling system. The sample tubes had a inner diameter of 3.5 mm.

III. Data Analysis and Simulations

Theory. For a two-pulse sequence $\pi/2$–τ–π–τ–echo, the echo amplitude for one $I = {}^1/_2$ nucleus (^{1}H, ^{31}P) is given by[10]

$$E_{mod}(\tau) = 1 - {}^1/_2k[1 - \cos(\omega_\alpha\tau) - \cos(\omega_\beta\tau) + {}^1/_2\cos((\omega_\alpha + \omega_\beta)\tau) + {}^1/_2\cos((\omega_\alpha - \omega_\beta)\tau)] \quad (1)$$

where ω_α and ω_β denote the nuclear transition (ENDOR) angular frequencies associated with the electronic states $m_s = {}^1/_2$ and $m_s = -{}^1/_2$, respectively, with[11]

$$\left|\begin{matrix}\omega_\alpha\\ \omega_\beta\end{matrix}\right| = [\tilde{l}(\pm\mathbf{A}/2 - \omega_n\mathbf{E})^2 l]^{1/2} \quad (2)$$

and the nuclear Zeeman angular frequency

$$\omega_n = g_n\beta_n B_0/\hbar \quad (3)$$

E is a 3 × 3 unit matrix, l is the unit vector along the static field B_0, and **A** is the hyperfine tensor (in units of radians per second) expressed in the molecular frame.

This coordinate system is particularly well suited for the calculation of ESEEM traces of powder samples. Furthermore, the approach is not restricted to point–dipole interactions but also allows for hyperfine couplings between the nuclei and a spatially distributed unpaired electron.

It can easily be shown that, for the sum frequency in eq 1, $\omega_\alpha + \omega_\beta \geq 2\omega_n$.[12] The shift $\Delta\omega = (\omega_\alpha + \omega_\beta) - 2\omega_n$ depends on the orientation of the nucleus with respect to B_0, the electron–nuclear distance r, and the isotropic hyperfine coupling a_{iso}. The modulation depth parameter k is defined by

$$k = 4\sin^2(\delta/2)\cos^2(\delta/2) \quad (4)$$

with

$$\left|\begin{matrix}\sin^2(\delta/2)\\ \cos^2(\delta/2)\end{matrix}\right| = \frac{|\omega_n^2 - {}^1/_4(\omega_\alpha \pm \omega_\beta)^2|}{\omega_\alpha\omega_\beta} \quad (5)$$

In eq 5, δ denotes the angle between the directions of the two effective magnetic fields at the nucleus for $m_s = {}^1/_2$ and $m_s = -{}^1/_2$.

The quantities $\cos^2(\delta/2)$ and $\sin^2(\delta/2)$ are proportional to the transition probabilities of the allowed and forbidden ESR transitions, indicating that both types of transitions are required for the observation of an echo modulation. According to eq 4, the modulation amplitudes are zero not only for isotropic but also for anisotropic spin systems with B_0 along one of the principal axes of the hyperfine tensor. In the formulae given above, the **g** tensor is assumed to be isotropic; extension of the expressions for an anisotropic **g** is straightforward.[12,13]

For nuclei with $I \geq 1$, the modulation formulas are much more complicated. Analytical expressions with various degrees of approximations including quadrupole interactions have been developed by several authors.[14-21] If only terms linear in k are considered and quadrupole couplings are neglected, eq 1 is still valid if k is replaced by $k' = {}^4/_3I(I+1)k$. However, it has been demonstrated by Dikanov et al.[22] that, with increasing I values, the term linear in k leads to an overestimation of the modulation depth. For ^{27}Al ($I = {}^5/_2$), higher order terms have to be considered for electron–nuclear distances $r < 0.4$ nm.

For spin systems consisting of n nuclei, the product rule[11,14]

$$E_{mod,n}(\tau) = \prod_{i=1}^{n} E_i(\tau) \quad (6)$$

applies. In polycrystalline samples, the modulation function is then given by

$$\langle E\rangle_{\theta,\phi} = 1/4\pi \int\int E_{mod,n}(\theta,\phi)\sin\theta\, d\theta\, d\phi \quad (7)$$

where the polar angles ϕ and θ describe the direction of B_0 with respect to the molecular frame.

Angular integration may be avoided if the multiplication in eq 6 is performed after integration for each nucleus. However, this approximation, known as the spherical model, is only valid for electron–nuclear distances $r \geq 0.4$ nm and $n \geq 4$.[10] For $r < 0.4$ nm, the modulation becomes sensitive to the geometrical arrangement of the different nuclei and eq 7 has to be applied.

Simulations. In order to get a *qualitative* picture of the spectral manifestations for the different types of coordinations between the ligands and the Cu(II) ion, a number of typical ESEEM patterns and the corresponding FT-ESEEM spectra have been calculated. The program SIMESEEM,[23] used for these computations, is based on the theory outlined above and allows one to calculate two- and three-pulse ESEEM patterns of disordered systems with an arbitrary number of nuclei and particular ranges ($\Delta\theta$, $\Delta\phi$) of the B_0 orientation. As input data, geometrical parameters obtained from X-ray or ENDOR studies on suitable model compounds or from chemical intuition have been used.

Since, in an ESEEM experiment, data acquisition is not possible for times τ shorter than the instrumental deadtime, $\tau_D \approx 100$–200 ns, modulations corresponding to hyperfine lines in the frequency domain with a width of $\Gamma \gtrsim 1/\tau_D$ are partially or even fully decayed within τ_D.[23-25] This is the reason that, in many ESEEM investigations on disordered systems, ω_α and ω_β transitions are not observed in the FT-ESEEM spectra and hyperfine splittings are inaccessible. For each type of nucleus the spectra often contain only the peaks near the sum frequency ($\omega_\alpha + \omega_\beta$) and a peak at ω_n caused by a large number of distant nuclei.[26] With a few exceptions, this is also the case for the systems studied in this work. In all the two-pulse ESEEM simulations shown below, a deadtime of τ_D = 200 ns is assumed.

The procedure to calculate the FT-ESEEM spectra is as follows. First, the nonmodulated part of the echo intensity, described by the constant term (1 − k/2) in eq 1, is subtracted from the modulation trace. Since no relaxation is used in the simulations, the damping of the modulation pattern is only caused by the powder average of the anisotropic contributions. After introduction of the deadtime, an exponential damping $e^{-a\tau}$ is applied, corresponding to the one found in the experimental ESEEM patterns after elimination of the background relaxation decay. Because of the truncation of the time domain data, only magnitude spectra will be presented. Window functions and extrapolation techniques into the deadtime region have not been used.

Since all experiments discussed in section IV have been performed with a B_0 field setting near the $g_\perp$ feature, the calculations of the powder average are restricted to $\theta = 90°$ and $0 < \phi < 180°$

(8) Fauth, J. M.; Schweiger, A.; Braunschweiler, L.; Forrer, J.; Ernst, R. R. *J. Magn. Reson.* **1986**, *66*, 74.
(9) Pfenninger, S.; Forrer, J.; Schweiger, A.; Weiland, Th. *Rev. Sci. Instrum.* **1988**, *59*, 752.
(10) Iwasaki, M.; Toriyama, K. *J. Chem. Phys.* **1985**, *82*, 5415.
(11) Kevan, L.; Schwartz, R. *Time Domain Electron Spin Resonance*; Wiley: New York, 1979.
(12) Iwasaki, M.; Toriyama, K.; Nunome, K. *J. Chem. Phys.* **1987**, *86*, 5971.
(13) Anderson, M. W.; Kevan, L. J. *Phys. Chem.* **1986**, *90*, 6452.
(14) Dikanov, S. A.; Tsvetkov, Yu. D. *J. Struct. Chem.* **1985**, *26*, 766.
(15) Ichikawa, T. *J. Chem. Phys.* **1985**, *83*, 3790.
(16) Shubin, A. A.; Dikanov, S. A. *J. Magn. Reson.* **1983**, *52*, 1.
(17) Shubin, A. A.; Dikanov, S. A. *J. Magn. Reson.* **1985**, *64*, 185.
(18) Rowan, L. G. *J. Magn. Reson.* **1987**, *74*, 308.
(19) Romanelli, M.; Narayana, M.; Kevan, L. *J. Chem. Phys.* **1985**, *83*, 4395.
(20) Romanelli, M.; Kevan, L. *J. Chem. Phys.* **1987**, *86*, 4369.
(21) Goldfarb, D.; Kevan, L. *J. Chem. Phys.* **1987**, *87*, 6323.
(22) Dikanov, S. A.; Shubin, A. A.; Parmon, V. N. *J. Magn. Reson.* **1981**, *42*, 474.
(23) Fauth, J.-M. Thesis, ETH, 1988.
(24) Astashkin, A. V.; Dikanov, S. A.; Tsvetkov, Yu. D. *Chem. Phys. Lett.* **1987**, *136*, 204.
(25) Fauth, J.-M.; Schweiger, A.; Ernst, R. R. *J. Magn. Reson.* **1989**, *81*, 262.
(26) Mims, W. B.; Peisach, J.; Davis, J. L. *J. Chem. Phys.* **1977**, *66*, 5536.

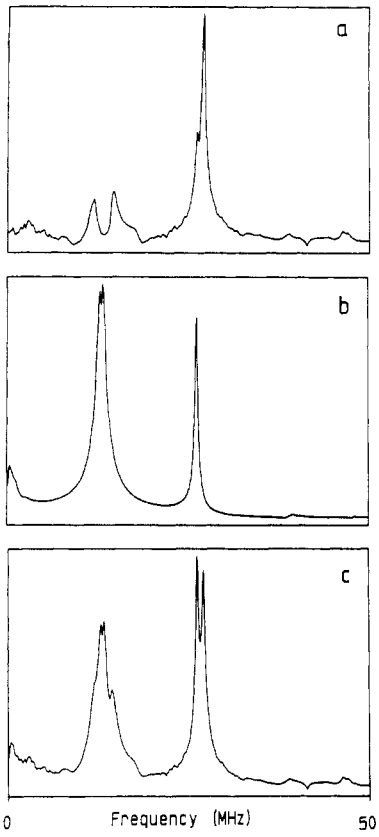

Figure 1. Calculated two-pulse FT-ESEEM magnitude powder spectrum of $Cu^{II}(H_2O)_6^{2+}$ (B_0 in the xy plane, proton Larmor frequency ν_H = 13 MHz, deadtime τ_D = 200 ns, geometrical parameters as discussed in text): (a) 12 local protons of directly coordinated water; (b) 12 protons of ambient water; (c) composite of spectrum a + 2.1(spectrum b).

(static field vector in the xy plane with B_0 = 0.3053 T (free proton frequency 13 MHz)).[13,21]

(A) Protons. The FT-ESEEM spectrum of a $Cu^{II}(H_2O)_6^{2+}$ complex in frozen aqueous solution is simulated by using single-crystal ENDOR data of Cu(II)-doped $Mg(NH_4)_2(SO_4)_2 \cdot 6H_2O$.[27] The magnitude spectrum of eight protons distributed in the complex plane (xy plane) with r = 0.257 nm (four equatorially coordinated water molecules) and four protons close to the complex normal with r = 0.28 nm (two axially coordinated water molecules) is shown in Figure 1a. The influence of ambient water on the spectrum is mimicked by 12 protons with r = 0.4 nm distributed on a sphere (Figure 1b). The two spectra are weighted and added, spectrum a + 2.1(spectrum b) = spectrum c (Figure 1c). This procedure corresponds to a linearization of eq 6, which is appropriate for small depth parameters as found for ambient water protons.

The doublet peak near 26 MHz in Figure 1c is characteristic for systems containing distant and local protons simultaneously. The sum frequency of the ambient and axial water protons is very close to twice the proton Larmor frequency $2\nu_H$ ($\omega_H = 2\pi\nu_H$), whereas the sum peak of the equatorial water proton is shifted to a higher frequency by about 1 MHz. Thus, this latter peak is indicative for the coordination of equatorial water in a square-planar copper complex. We will refer to this typical spectral feature in section IV.

(B) Distant Phosphorus. To mimic the phosphorus modulation in an outer-sphere coordination between copper ions and phosphates, the ESEEM pattern of one ^{31}P nucleus in the xy plane with r = 0.45 nm is calculated. Figure 2a shows the untreated ESEEM pattern without relaxation. The modulation with frequency $\nu_P \approx \nu_\alpha \approx \nu_\beta$ ($\omega_\alpha = 2\pi\nu_\alpha$; $\omega_\beta = 2\pi\nu_\beta$) decays within about 2 μs because of the anisotropy of the weak hyperfine coupling; the sum frequency $\nu_\alpha + \nu_\beta \approx 2\nu_n$ is not essentially damped.

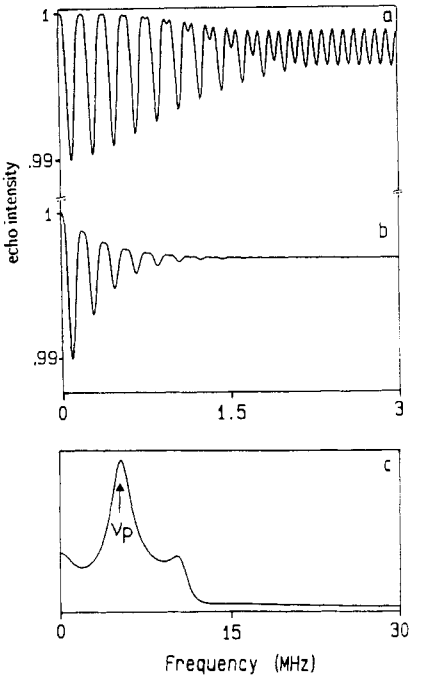

Figure 2. Calculated two-pulse ESEEM of one distant phosphorus nucleus (B_0 and phosphorus nucleus in the xy plane, r = 0.45 nm): (a) modulation pattern, modulation depth ≈1%; (b) modulation pattern (without constant term) damped by the exponential decay function e^{-ar}, a = 3.3 MHz, which corresponds to the damping found experimentally in the ESEEM pattern of Cu^{II}(glucose phosphate) in frozen solution; (c) FT-ESEEM magnitude powder spectrum of (b) (τ_D = 200 ns). The peak of the phosphorus Larmor frequency ν_P = 5.3 MHz is the dominant feature.

Elimination of the constant echo intensity and application of a damping typically found in the frozen-solution samples (see Figure 6a) results in the ESEEM trace shown in Figure 2b. Fourier transformation of this ESEEM trace yields the magnitude spectrum given in Figure 2c. Since the modulation depth is very small (≈1%), only a weak phosphorus peak at ν_P is expected for an outer-sphere complexation.

(C) Vicinal Phosphorus. Next, we consider the phosphorus modulations of two bidentate phosphate ligands coordinated in equatorial position to the copper ion. The four phosphorus nuclei and the copper ion are assumed to lie in a plane tilted by 20° from the complex plane ($g_\perp$) with a copper–phosphorus distance of r = 0.3 nm and isotropic hyperfine couplings a_{iso} of 0, 1.5, 3, and 4.5 MHz. Apart from the copper–phosphorus distance, these data are obtained by chemical intuition, since experimental values are not available. The untreated ESEEM pattern and the corresponding FT-ESEEM spectrum are shown in Figure 3a,b. The spectrum is dominated by the sum peak near $2\nu_P$ = 10.5 MHz. The peaks ν_α and ν_β containing the hyperfine information are very weak, as a result of the deadtime of 200 ns, and spread over several megacycles. In an experimental spectrum they will usually be buried in the noise.

As a rule, in spin systems with several close nuclei of different coupling parameters only the sum peak is observed, whereas for distant nuclei the peak near the Larmor frequency is the dominant feature in the FT-ESEEM spectrum.

The simulation of a special case of a ^{31}P coupling motivated by the experimental data observed on Cu^{II}(pyrophosphate)$_2$ is given in Figure 3c. The same parameters as in the former case are used with the exception that a_{iso} = 8.2 MHz. Only the ν_α and ν_β transitions are plotted. The upper trace in Figure 3c shows the cosine transform spectrum with τ_D = 0. The ν_α frequencies are close to zero, whereas the ν_β frequencies near 10 MHz with the unusual shape[28] overlap with the sum peak $\nu_\alpha + \nu_\beta$ *and* the difference peak $\nu_\beta - \nu_\alpha$. By introduction of a deadtime of τ_D =

(27) Atherton, N. M.; Horsewill, A. J. *Mol. Phys.* **1979**, *37*, 1349.

(28) de Groot, A.; Evelo, R.; Hoff, A. J. *J. Magn. Reson.* **1986**, *66*, 331.

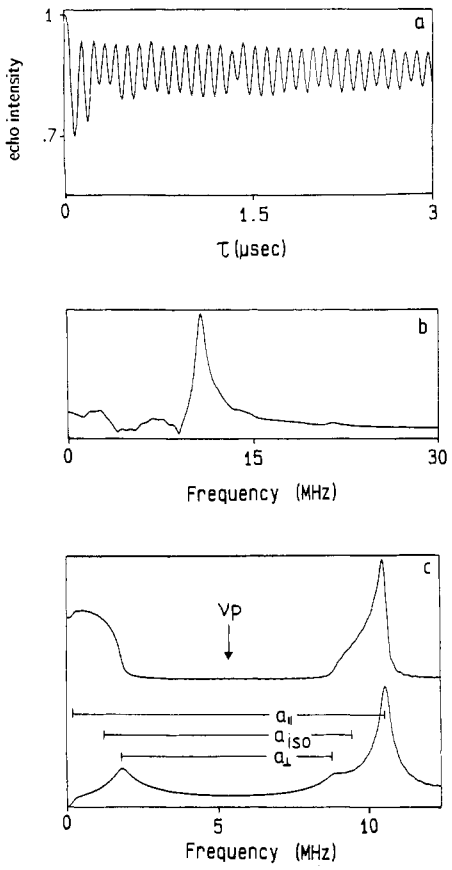

Figure 3. (a) Calculated two-pulse ESEEM of four vicinal phosphorus nuclei with isotropic hyperfine couplings ranging from 0 to 4.5 MHz (B_0 in the xy plane, r = 0.3 nm). (b) FT-ESEEM magnitude spectrum of (a). Due to the truncation of the time domain data (τ_D = 200 ns), essentially only the peak at twice the ^{31}P Larmor frequency $2\nu_P$ = 10.6 MHz is observed. (c) Demonstration of the influence of the deadtime on a two-pulse FT-ESEEM powder spectrum. To emphasize the crucial points, sum and difference peaks are omitted (r = 0.3 nm, a_{iso} = 8.2 MHz, B_0 in the xy plane). Upper trace: τ_D = 0, cosine transform spectrum. Lower trace: τ_D = 200 ns, magnitude spectrum.

200 ns and computation of the magnitude spectrum, only a peak at 2 MHz, corresponding to $\nu_P - A_\perp/2$ and a peak at 10.6 MHz $\approx \nu_\alpha + \nu_\beta$ ($\nu_P + A_\parallel/2$) survive this truncation of the data (lower trace). The feature at $\nu_P + A_\perp/2$ is only poorly resolved. This example demonstrates that one should be very careful with the evaluation of data from peak maxima in FT-ESEEM spectra.

(D) Aluminum. For various reasons the simulation of aluminum ESEEM patterns is a difficult task.[19-21] First, higher order terms in the depth parameter have to be included in the computation because of the large spin quantum number $I = {}^5/_2$. Second, the isotropic hyperfine and the nuclear quadrupole couplings may strongly affect the ESEEM patterns; both interactions are usually not known. In particular the quadrupole interaction tensors defined by five unknown parameters can alter the modulation substantially.[21] Finally, many aluminum nuclei in different positions may be coupled to the unpaired electron. This is especially true in our study where the copper ion interacts with a large number of aluminum nuclei of the δ-Al_2O_3 framework.

In order to get a rough estimate of aluminum ESEEM patterns of surface complexes, four model types of coordination of the copper ion to the hydrous oxide surface are considered (Scheme I): (a) outer-sphere complex with an end-on O^- ion; (b) outer-sphere complex with a bridged O^- ion; (c) inner-sphere complex with an end-on O^-; (d) inner-sphere complex with a bridged and end-on O^-.

A face-centered cubic structure is assumed for δ-Al_2O_3. Due to the lack of corresponding data, a_{iso} and the quadrupole couplings are neglected. Since the modulation is dominated by aluminum nuclei close to the copper center, different upper limits of electron–nuclear distances have been taken into account in the simulations. The two-pulse ESEEM patterns without decay and the corresponding magnitude spectra for the four cases are shown in Figure 4. Prior to Fourier transformation, a decay of the modulation trace is introduced, again adapted from the experimental data. The decay in the case of these surface complexes is faster than in the case of complexes in frozen solutions (compare Figure 11a with Figure 6a), resulting in broader features in the frequency domain.

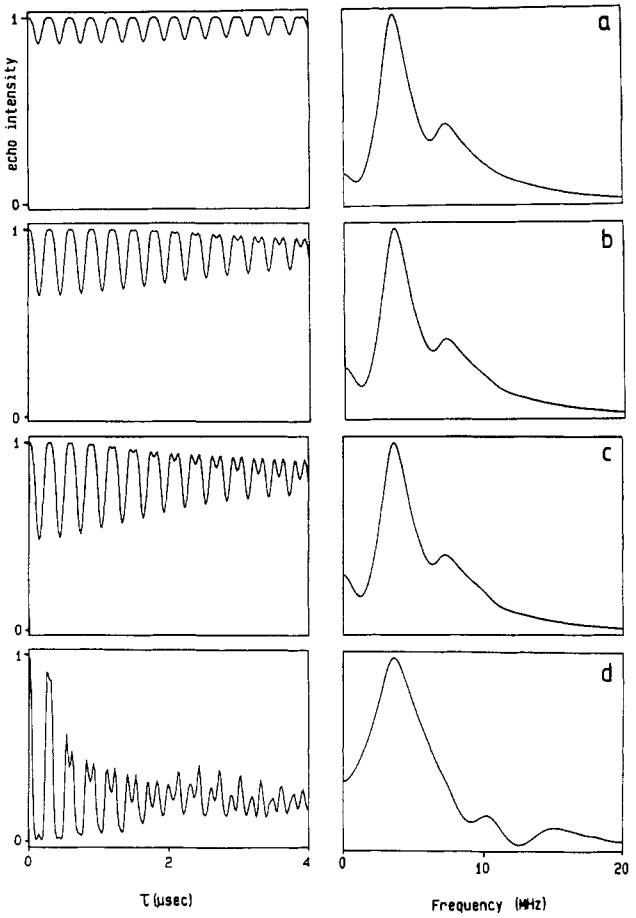

Figure 4. Calculated two-pulse ESEEM of ^{27}Al nuclei in the first two layers of δ-Al_2O_3 for four different types of Cu(II) coordination: (left) ESEEM trace; (right) FT-ESEEM magnitude powder spectra. The damping function used prior to the Fourier transformation was $e^{-a\tau}$, a = 5.3 MHz. Positions (ϕ, θ, r) of the aluminum nuclei are based on the structures and the coordinate system given in Scheme I. Distances: Al–O = 0.2 nm; O···H = 0.2 nm; O–H = 0.1 nm; Cu–O = 0.2 nm. Angles: ∠(OH) = 109.5°; ∠(Cu–O) = 90°. (a) Eight aluminum nuclei of Scheme Ia (first layer), r_{max} < 0.7 nm. ϕ, θ, r: 168°, 90°, 0.569 nm; 188°, 70°, 0.596 nm; 188°, 110°, 0.596 nm; 207°, 90°, 0.622 nm; 150°, 107°, 0.673 nm; 150°, 73°, 0.673 nm; 168°, 120°, 0.696 nm; 168°, 60°, 0.696 nm. (b) Eight aluminum nuclei of Scheme Ib (first layer), r_{max} < 0.65 nm. ϕ, θ, r: 161°, 90°, 0.478 nm; 186°, 66°, 0.496 nm; 186°, 114°, 0.496 nm; 208°, 90°, 0.514 nm; 142°, 109°, 0.609 nm; 142°, 71°, 0.609 nm; 161°, 50°, 0.623 nm; 161°, 130°, 0.623 nm. (c) Nine aluminum nuclei of Scheme Ic (first layer), r_{max} < 0.6 nm. ϕ, θ, r: 180°, 90°, 0.4 nm; 153°, 66°, 0.49 nm; 207°, 66°, 0.49 nm; 153°, 114°, 0.49 nm; 207°, 114°, 0.49 nm; 135°, 90°, 0.566 nm; 180°, 45°, 0.566 nm; 225°, 90°, 0.566 nm; 180°, 135°, 0.566 nm. (d) Seventeen aluminum nuclei of Scheme Id (first and second layer), r_{max} < 0.5 nm. ϕ, θ, r: 180°, 45°, 0.283 nm; 225°, 90°, 0.283 nm; 180°, 135°, 0.283 nm; 135°, 90°, 0.283 nm; 180°, 90°, 0.4 nm; 225°, 35°, 0.49 nm; 243°, 66°, 0.49 nm; 243°, 114°, 0.49 nm; 225°, 145°, 0.49 nm; 135°, 145°, 0.49 nm; 116°, 114°, 0.49 nm; 116°, 66°, 0.49 nm; 135°, 35°, 0.49 nm; 154°, 67°, 0.49 nm; 207°, 67°, 0.49 nm; 207°, 114°, 0.49 nm; 154°, 114°, 0.49 nm.

Apart from the modulation depth, the ESEEM patterns of the structures a–c look rather similar. The small differences in the modulation depth of structures b and c indicate that a discrimination between these inner- and outer-sphere complexes based on the aluminum modulations might be difficult. The pattern of complex d, however, is completely different from the former ones. This is due to the coupling of the nearest aluminum nuclei

Table I. ESR Parameters and Types of Coordination ($A_{\parallel}^{Cu}$ in 10^{-4} cm^{-1})

	in frozen solutions			in presence of δ-Al_2O_3		
system	$g_{\parallel}$ (±0.005)	$A_{\parallel}^{Cu}$ (±1)	type of phosphate coord	$g_{\parallel}$ (±0.005)	$A_{\parallel}^{Cu}$ (±1)	type of surface coord
Cu^{II}(aquo) complex	2.41	147		2.36	165	^{27}Al inner-sphere
Cu^{II}(orthophosphate)			insoluble ppt ($\log K_{so} = -36.9$)	2.36	156	^{27}Al inner-sphere; phosphate not coordinated to Cu(II)
Cu^{II}(pyrophosphate)$_2$	2.38	161	inner-sphere	2.36	148	^{27}Al inner-sphere; phosphate not coordinated to Cu(II)
Cu^{II}(tripolyphosphate)	2.39	149	inner-sphere	2.35	167	^{27}Al inner-sphere; phosphate not coordinated to Cu(II)
Cu^{II}NTP	2.32	145	inner-sphere	2.32	159	ternary inner-sphere surface complex with Cu(II)
Cu^{II}(glucose phosphate)	2.43	150	outer-sphere			

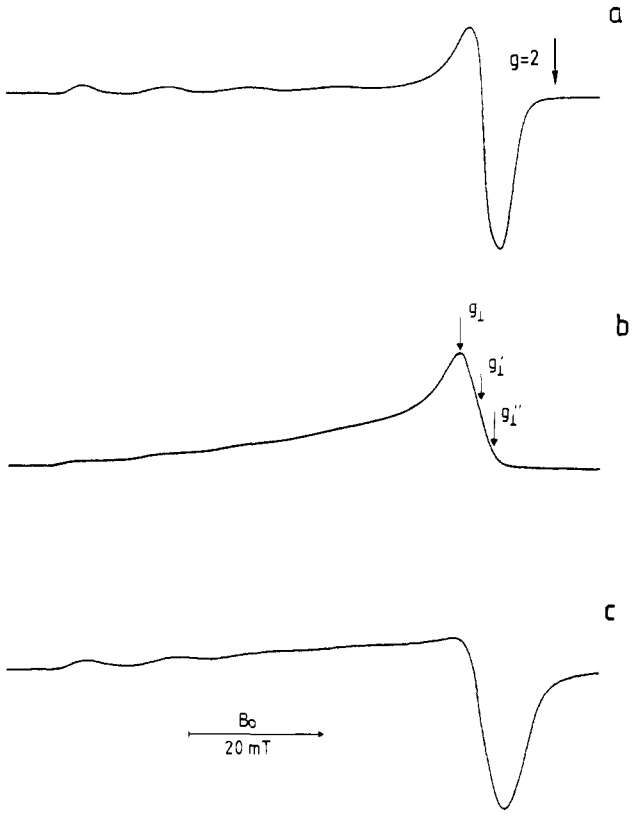

Figure 5. (a) ESR spectrum of Cu^{II}(pyrophosphate)$_2$ in frozen solution at T = 90 K. (b) Integrated spectrum. Arrows indicate observer positions used in the ESEEM experiments. (c) ESR spectrum of Cu^{II}(pyrophosphate)$_2$ adsorbed on δ-Al_2O_3 at T = 90 K.

Scheme I

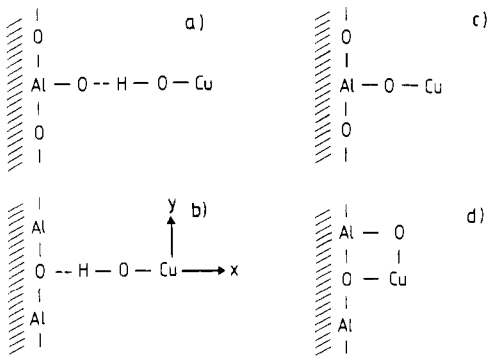

with electron–nuclear distances as short as r = 0.283 nm. This distance causes a 100% modulation effect for short τ values and a diminution of the echo to about one-third of its maximum intensity for $\tau > 2\mu s$.

IV. Results

(A) ESR Spectra. Two ESR spectra representative of a copper phosphate complex in frozen solution and a copper surface complex are shown in Figure 5. The arrows in the integrated frozen-solution spectrum (Figure 5b) indicate the observer positions at the peak maximum ($g_\perp$), at half-height ($g_\perp'$), and at the high-field end of the spectrum ($g_\perp''$).

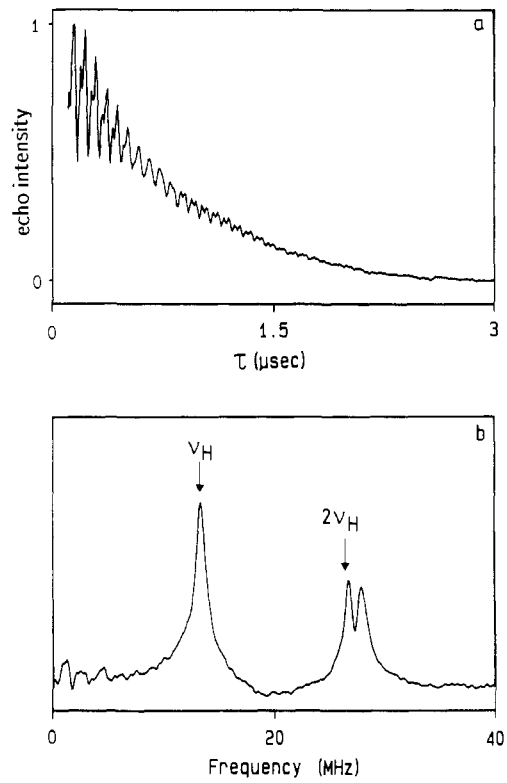

Figure 6. (a) Two-pulse ESEEM of Cu^{II}(aquo) complex in frozen glycerol/H_2O solution at T = 10 K. (b) FT-ESEEM magnitude spectrum of (a), ν_H = 13.4 MHz.

The line width of the surface complexes is found to be considerably broader than that of the copper complexes in frozen solutions. This is attributed to larger strain effects[29] caused by the poorly defined structure of the δ-Al_2O_3 surface. The magnetic parameters $g_{\parallel}$ and $A_{\parallel}^{Cu}$ summarized in Table I, however, are very similar for all compounds studied in this work. This is so much more the case for the $g_\perp$ values ($g_\perp \approx 2.07$). Since **g** tensors of copper complexes are often slightly orthorhombically distorted and the resolution of the ESR spectra is quite poor, $g_\perp$ values are not included in Table I. Obviously, detailed information concerning the type of coordination may not be extracted from these ESR data.

(B) ESEEM of Frozen Solutions. Cu^{II}(aquo) Complex. Two-pulse modulations of the Cu^{II}(aquo) complex have been measured at positions $g_\perp$, $g_\perp'$, and $g_\perp''$. The ESEEM pattern and the corresponding FT-ESEEM spectrum along $g_\perp$ are shown in Figure 6. The results are similar to those obtained by Mims et al.[26] The strong sum peak at 27.8 MHz is due to equatorial water protons whereas the peak close to twice the proton Larmor

(29) Hagen, W. R. *J. Magn. Reson.* **1981**, *44*, 447.

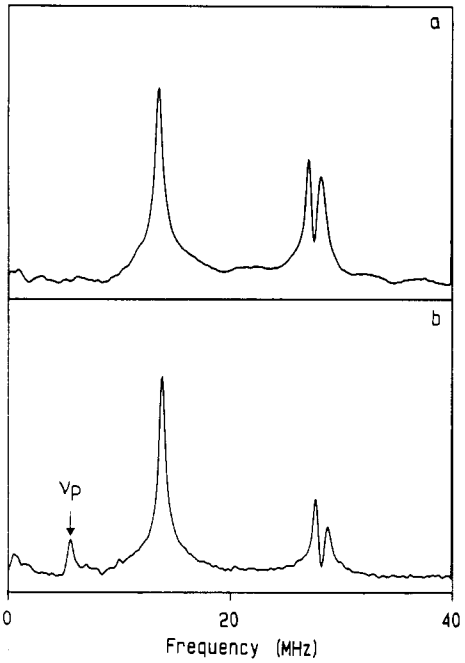

Figure 7. Two-pulse FT-ESEEM magnitude spectra of Cu^{II}(glucose phosphate) in frozen solution at T = 10 K: (a) B_0 position $g_\perp$; (b) B_0 position $g_\perp''$ (arrow marks the peak at the ^{31}P Larmor frequency).

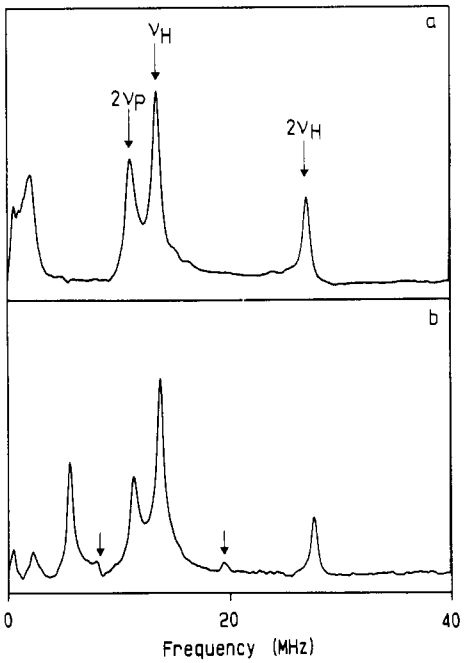

Figure 8. Two-pulse FT-ESEEM magnitude spectra of Cu^{II}(pyrophosphate)$_2$ in frozen solution at T = 10 K: (a) B_0 position $g_\perp$; (b) B_0 position $g_\perp''$ (arrows mark combination lines $\nu_H + \nu_P$ and $\nu_H - \nu_P$).

frequency $\nu_H = \omega_H/2\pi$ results from axially coordinated and ambient water protons (see Figure 1).

Cu^{II}(glucose phosphate). The FT-ESEEM spectra of Cu^{II}(glucose phosphate) measured at $g_\perp$ and $g_\perp''$ are displayed in Figure 7. For B_0 at position $g_\perp$ (Figure 7a), the results are similar to those of the Cu^{II}(aquo) ion. At $g_\perp''$ (Figure 7b), however, a weak peak at the phosphorus Larmor frequency ν_P = 5.7 MHz is observed, indicating that a loosely coupled ^{31}P nucleus is present (see Figure 2). The reason that the ^{31}P peak is only detectable at the high-field end of the ESR spectrum is due to the improved orientation selection attainable at this observer position. Note that also the resolution of the proton doublet near $2\nu_H$ is improved. This effect, which is well-known from ENDOR[30] spectroscopy on transition-metal complexes with strongly anisotropic magnetic interactions, can also lead to a drastic resolution enhancement in FT-ESEEM spectra (see below).

Cu^{II}(pyrophosphate)$_2$. Figure 8 shows the FT-ESEEM spectra of Cu^{II}(pyrophosphate)$_2$ again measured at $g_\perp$ and $g_\perp''$. Only one proton sum peak is observed, indicating that no equatorially coordinated water is present. The sum peak near $2\nu_H$ is due to protons of ambient and axially coordinated water. The strong sum peak of ^{31}P at $2\nu_P \approx 11.2$ MHz refers to local phosphorus nuclei (see Figure 3b). According to X-ray data on sodium copper pyrophosphate hexadecahydrate,[31] the copper–phosphorus distance is about 0.31 nm. The broad transition observed for $g_\perp$ with a peak maximum at 2.1 MHz is assigned to one of the ^{31}P hyperfine lines truncated by the deadtime. According to the simulation shown in Figure 3d, this peak is considered as the $(\nu_P - A_\perp/2)$ transition, resulting in an isotropic coupling of a_{iso} = 8.2 MHz. The peak $\nu_P + A_\parallel/2$ approximately coincides with the sum peak, so that spectral features from the high-frequency transition will be difficult to observe. For $g_\perp''$, again a peak at the phosphorus Larmor frequency of ν_P = 5.6 MHz is found, indicating the presence of more distant phosphorus nuclei. We assume that some of the excess phosphorus ligand (molar ratio Cu:phosphate = 1:3) may coordinate axially to the copper ion. The two peaks marked by arrows are combination lines with frequencies $\nu_H + \nu_P$.

Cu^{II}(tripolyphosphate). The experimental results obtained for Cu^{II}(tripolyphosphate) are given in Figure 9 (molar ratio Cu:phosphate = 1:1). Apart from peaks at the proton and phosphorus

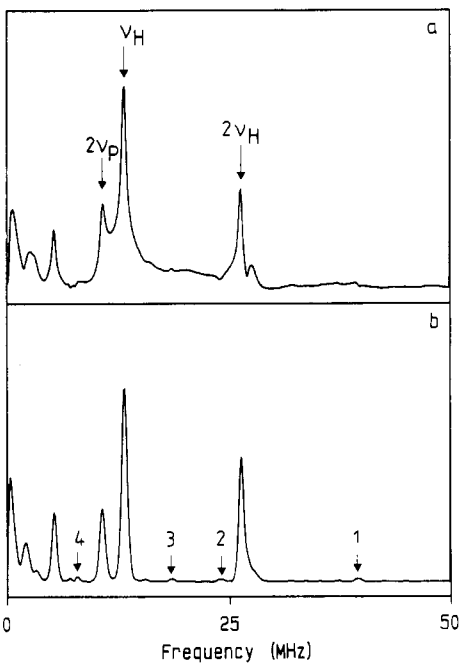

Figure 9. (a) Two-pulse FT-ESEEM magnitude spectrum of Cu^{II}(tripolyphosphate) in frozen solution at T = 10 K, B_0 position $g_\perp$. (b) Spectrum for same solution as in (a) except prior to Fourier transformation an apodization procedure has been applied (Hanning window with τ_{max} = 4 μs). Arrows mark the following combination lines: (1) $3\nu_H$; (2) $\nu_H + 2\nu_P$; (3) $\nu_H + \nu_P$; (4) $\nu_H - \nu_P$.

Larmor frequencies, the FT-ESEEM spectrum in Figure 9a (observer position $g_\perp$) shows the proton sum peak of presumably two equatorial water molecules at 27.5 MHz and the ^{31}P sum peak at 10.7 MHz of the local phosphorus nuclei. In contrast to Cu^{II}(pyrophosphate)$_2$ the peak at the Larmor frequency of ^{31}P is already present for a B_0 field at $g_\perp$. It has to be concluded that this peak is due to the coupling of the third (remote) ^{31}P nucleus of tripolyphosphate. The peak at 2.6 MHz may be part of the ν_α transition of ^{31}P. The feature is, however, much less pronounced than the one in Cu^{II}(pyrophosphate)$_2$. The isotropic hyperfine interactions are probably not the same for the two local phosphorus nuclei, resulting in a broader ν_α transition, which is strongly reduced in intensity by the deadtime.

(30) Van Camp, H. L.; Scholes, C. P.; Mulks, C. F.; Caughey, W. S. *J. Am. Chem. Soc.* **1977**, *99*, 8283.
(31) Yuen, P.; Collin, R. L. *Acta Crystallogr., Sect. B* **1974**, *30*, 2513.

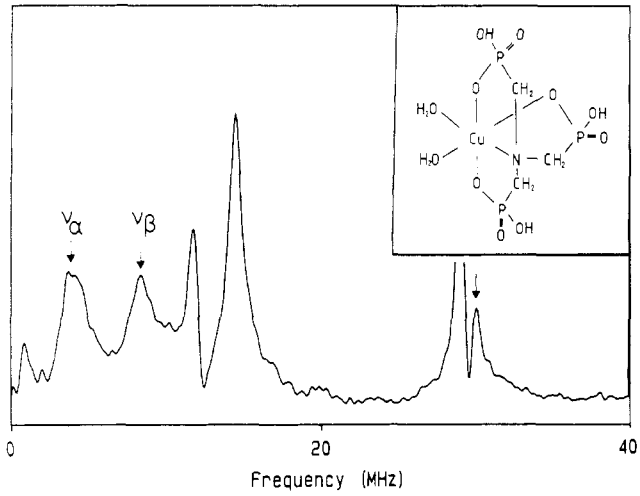

Figure 10. Two-pulse FT-ESEEM magnitude spectrum of $Cu^{II}NTP$ in frozen solution at $T = 10$ K, B_0 position $g_\perp''$. Arrows mark ^{31}P hyperfine lines ν_α and ν_β and the sum peak of the equatorially coordinated water protons. Insert: Structure of $Cu^{II}NTP{\cdot}2H_2O$.

Figure 9b demonstrates the influence of a Hanning window $h(\tau) = 0.5–0.5 \cos(2\pi\tau/\tau_{max})$ on the FT-ESEEM spectrum.[32] The resolution is drastically improved, and several combination peaks (marked by numbers) are now clearly visible. Note, however, that features like the sum peak of the equatorial water protons can get lost by using such a tapering of the data.

Similar spectra are obtained for Cu^{II}(tripolyphosphate)$_2$. Equatorial water protons are no longer observed, and the intensity ratio $I(2\nu_P):I(\nu_H)$ has increased, indicating that more local phosphorus nuclei are present.

$Cu^{II}NTP$. Figure 10 shows the FT-ESEEM spectrum of $Cu^{II}NTP$ recorded at $g_\perp''$. The spectrum is well resolved, and there is no need for a tapering of the data. NTP is a tetradentate ligand, so that water is only coordinated at the two remaining positions. This is confirmed by the pronounced sum peak at 30.0 MHz (arrow). Since the complex is tetragonally distorted, the terminology "equatorial" and "axial" no longer strictly applies for the water protons. The ^{31}P spectrum consists of a narrow phosphorus sum peak at 11.8 MHz and two well-developed hyperfine lines $\nu_\alpha = 3.9$ MHz and $\nu_\beta = 8.4$ MHz (arrows). Considering the influence of the deadtime, an isotropic hyperfine coupling of 5–6 MHz is found. These two peaks are not observed at $g_\perp$ and are only poorly developed at $g_\perp'$. This again demonstrates that a proper orientation selection may be essential to get optimum results. We assign this coupling to the ^{31}P nucleus in the complex plane.

(C) ESEEM of Surface Complexes. Aqueous solutions of $Cu^{II}(H_2O)_6^{2+}$, Cu^{II}(orthophosphate), Cu^{II}(pyrophosphate) (CuL, CuL_2), and Cu^{II}(tripolyphosphate) (CuL, CuL_2) in the presence of δ-Al_2O_3 form surface complexes. This is manifested by the strong aluminum modulation observed in all of these compounds. The ESEEM pattern and the FT-ESEEM spectrum of Cu(II)–δ-Al_2O_3 are shown in Figure 11.

Very similar spectra have been recorded for the copper–phosphate complexes mentioned above. The echo decays of these surface compounds are much faster than those for the complexes in frozen solutions (see Figure 6a). We assume that the Cu(II) ions on the surface are not so well separated from each other as in frozen aqueous/glycerin solutions, resulting in a shortening of the phase memory time. The most striking observation is the fact that phosphorus modulations do not occur in these FT-ESEEM spectra. This proves that the phosphates are no longer coordinated to the copper ion. However, all spectra show a prominent sum peak due to equatorial water protons. Thus, in the presence of δ-Al_2O_3 the phosphate ligands are directly coordinated to the surface rather than to the copper ions. The aluminum peak at

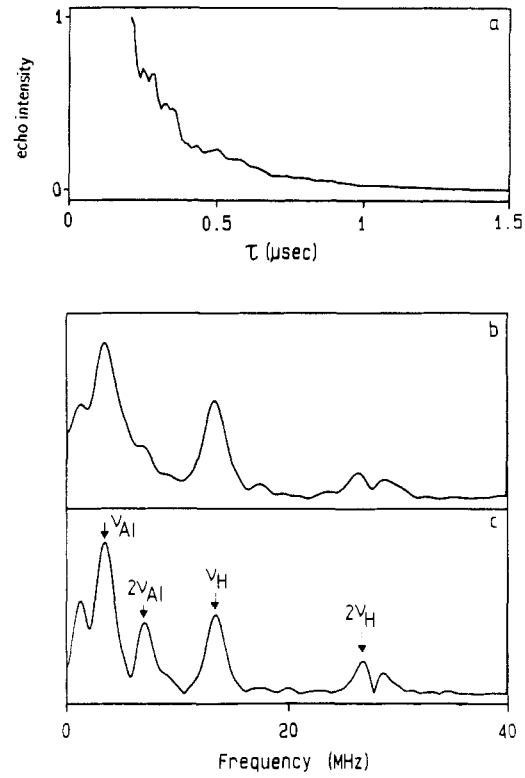

Figure 11. Two-pulse ESEEM of Cu(II) adsorbed on δ-Al_2O_3 at $T = 10$ K, B_0 position $g_\perp$: (a) ESEEM pattern; (b) FT-ESEEM magnitude spectrum; (c) spectrum as in (b) except prior to Fourier transformation an apodization procedure has been applied (Hanning window with $\tau_{max} = 1.2$ μs).

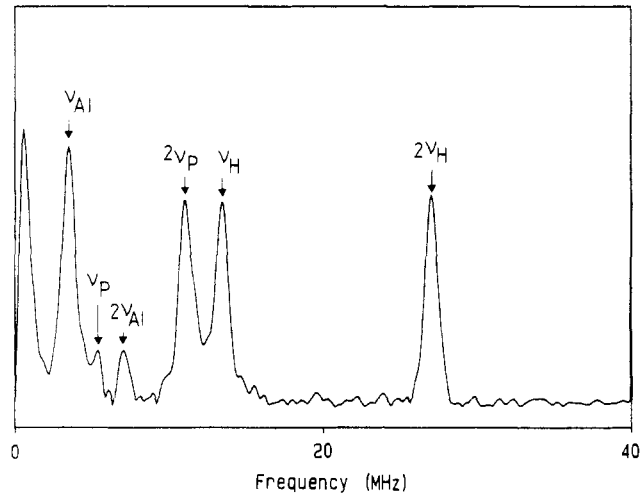

Figure 12. Two-pulse FT-ESEEM magnitude spectrum of $Cu^{II}NTP$ on δ-Al_2O_3 at $T = 10$ K, B_0 position $g_\perp$. Prior to Fourier transformation, an apodization procedure has been applied (Hanning window with $\tau_{max} = 3$ μs).

the aluminum Larmor frequency of $\nu_{Al} = 3.4$ MHz is the dominant feature in the spectrum (Figure 11b). A somewhat weaker peak is observed at the position of the sum frequency. Again, Hanning windowing of the time domain data essentially improves the resolution (Figure 11c).

It is difficult to decide from the depth of the aluminum modulation whether copper forms an inner- or outer-sphere coordination with the surface of δ-Al_2O_3. A coordination according to type d in Scheme I, however, can be excluded.

A different situation is found for $Cu^{II}NTP$. The FT-ESEEM spectrum displayed in Figure 12 (B_0 position $g_\perp$) shows proton, aluminum, and phosphorus peaks. Again apodization prior to Fourier transformation has been applied. A sum peak of equatorial protons is not observed (with or without apodization). This strongly indicates that the two water ligands are replaced by

(32) Merks, R. P. J.; de Beer, R. *J. Magn. Reson.* **1980**, *37*, 305.

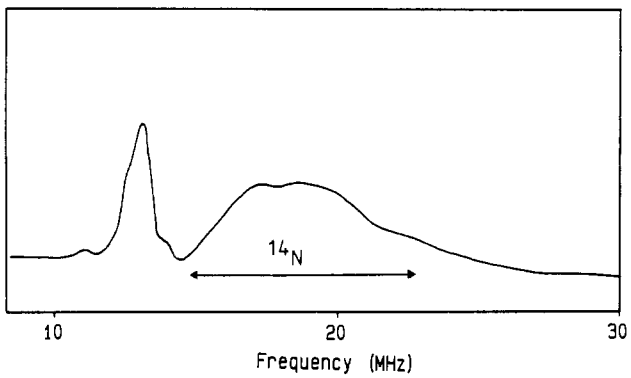

Figure 13. cw-ENDOR spectrum of $Cu^{II}NTP$ adsorbed on δ-Al_2O_3 at T = 10 K, B_0 position $g_\perp$. The broad line between 15 and 23 MHz is due to the nitrogen ligand directly coordinated to Cu(II).

functional groups of the δ-Al_2O_3 surface, resulting in an inner-sphere coordination.

Since a strong ^{31}P sum peak and a weak peak at ν_P are present, NTP is still directly coordinated to the Cu(II) ion (see Figure 10). Thus, Cu(II) forms a ternary complex with NTP and the δ-Al_2O_3 surface. The aluminum modulation depths are similar to those of the other Cu(II) ions on δ-Al_2O_3. Therefore, we assume that, for all compounds investigated in this work, the Cu(II) ion forms an inner-sphere coordination with δ-Al_2O_3.

Moreover, coordination of NTP to the copper ion is proved by the cw-ENDOR spectrum (Figure 13), which shows a broad line between 15 and 23 MHz typical of a directly coordinated nitrogen ligand.

V. Discussion

The formation of phosphate complexes with Cu(II) is adequately characterized by the determination of thermodynamic stability constants. Such data do not directly lead to information with respect to the molecular structure of the formed coordination compounds. Therefore, the analysis of established equilibria of complex formation in solution and adsorption isotherms on surfaces is complemented by ESR spectroscopic methods.

(A) Copper(II) Complexes with Inorganic Phosphates in Aqueous Solutions. Orthophosphate readily forms sparingly soluble precipitates with most heavy metal ions (the solubility product of $Cu_3(PO_4)_2$ is characterized by log $K_{so} \approx -36.9$[33]), and it is generally not possible to determine the structure of the solution species (for Cu(II) the concentration of the complex is smaller than 10^{-7} M). It is for this reason that no ESR signal is detectable that could be assigned to a solution $Cu^{II}PO_4$ complex. Pyrophosphate and tripolyphosphate in contrast to orthophosphate form very stable Cu(II) complexes in solution (log $K_1 \approx 7.6$ and log $K_1 \approx 9.0$, respectively[33]) due to bidentate chelation.

This is corroborated by the analysis of the ESEEM spectrum of Cu^{II}(pyrophosphate)$_2$, which exhibits a pronounced ^{31}P peak at $2\nu_P$, indicative of the proximity of the phosphorus nuclei. Furthermore, ligation takes place within the equatorial plane of the tetragonal environment of Cu(II) that has been shown in the previous analysis of the ^1H features of the spectrum.

Cu^{II}(tripolyphosphate) shows a different FT-ESEEM spectrum due to the fact that $P_3O_{10}^{5-}$ acts as a bidentate ligand comprised of two inner-sphere P–O functional groups linked to the Cu(II) center, leaving one outer-sphere P–O functional group as indicated in Figure 9 by the peak at Larmor frequency ν_P. The sum peak of the protons of equatorial water ligands disappears upon formation of Cu^{II}(tripolyphosphate)$_2$ (spectrum not shown in this work).

In conclusion the FT-ESEEM spectra are fully consistent with the configuration of complexes derived from thermodynamic data.

(B) Cu^{II}(glucose phosphate). Glucose phosphate was chosen as a representative example for a single terminal functional group, since monophosphate derivatives as a result of glycolysis in the energy-transfer metabolism of living systems are a widespread class of molecules in the phosphorus transformation cycle. Contrary to PO_4^{3-}, glucose phosphate does not readily form precipitates with Cu(II); however, it is bound to the Cu^{II}(aquo) ion by an ion association mechanism in neutral aqueous medium. ESEEM data indicate that the hydration sphere of the Cu^{II}(aquo) ion is completely retained as shown in section IVB). The signal at the phosphorus Larmor frequency ν_P = 5.7 MHz is evidence for an outer-sphere type of bonding to the Cu^{II}(aquo) ion. The association behavior of glucose phosphate is in marked contrast to the inorganic phosphates complex formation properties as discussed in section VA).

(C) $Cu^{II}NTP$. Tetradentate coordination of the ligand NTP to Cu(II) is substantiated by the analysis of ENDOR and FT-ESEEM spectra. Whereas the strong isotropic hyperfine coupling prevents the formation of an ^{14}N ESEEM, two sets of ^{31}P signals can be observed assignable to one "equatorial" and two "axial" positions, although the ESR parameters (cf. Table I) indicate a certain distortion from a strict tetragonal configuration.[34,35]

(D) Surface Complexes on Hydrous δ-Al_2O_3. The affinity of heavy metals for adsorption on hydrous oxide surfaces is strongly influenced by pH and other ligands dissolved.[36] Many cases of enhanced metal adsorption have been reported as due to the presence of sulfates, phosphates, and other ligands. Ternary surface complex formation e.g. of Cu(II) with various anions has been demonstrated to influence the overall stability of the metal complex.[37] However, for anions (SO_4^{2+}, Cl^-, PO_4^{3-}) that themselves have a high tendency to be adsorbed by hydrous metal oxides, there is no clear-cut evidence of mutual interactions between the metal cation and the ligand anion in the adsorbed state.

The strategy behind this study was to investigate (by the specific spectroscopic techniques of ESEEM) the underlying bonding mechanism in a system that is characterized by strong complex formation capacity of all the constituents in solution as well as onto the surface of hydrous δ-Al_2O_3. the most striking result of this study is the observation that all the *inorganic phosphate complexes of Cu(II) dissociate* upon adsorption and no ternary complexes are formed under the experimental conditions chosen. ESR and ESEEM data unambiguously show the features of Cu(II) bound to the surface functional groups of ≡Al–O. However, the analysis of the aluminum modulation does not allow one to discriminate between different types of binding (see Scheme I and the data analysis in section IVC). No signals due to ^{31}P interactions are present; i.e., the phosphate ligands are bound to the surface of aluminum on separate sites. Precipitation of Cu^{II}(phosphate) can be prevented in the presence of δ-Al_2O_3, and Cu(II) again is held as a surface complex of the type $(\equiv AlO)_2Cu$, whereas phosphate probably is adsorbed as an inner-sphere binuclear complex of the type ≡Al–O–(O)P(O)–O≡Al.[38]

The organophosphate complex $Cu^{II}NTP$ in contrast to the above described situation does not dissociate upon adsorption. As shown in the FT-ESEEM analysis, an inner-sphere ternary surface complex of the type $(\equiv AlO)_2Cu^{II}NTP$ can be deduced combining all the elements of the spectral parameters analysis. This characteristic of the NTP ligand could possibly be accounted for its higher complex stability of Cu(II) over that of Al(III); generally, stability constants of surface complexes with hydrous oxides follow the trend of their solution counterparts.[39]

Acknowledgment. This project has been supported by a grant from the Board of the Swiss Federal Institutes of Technology. We are grateful to Jean-Michel Fauth for valuable assistance and to Barbara Sulzberger for sample preparations.

(33) Sillen, L. C.; Martell, A. E. *Stability Constants of Metal-Ion Complexes*; Special Publication 17 & Suppl.; The Chemical Society: London, 1971; Vol. 1; p 25.
(34) Hathaway, B. J. *J. Chem. Soc. A* **1969**, 316.
(35) Peisach, J.; Blumberg, W. E. *Arch. Biochem. Biophys.* **1974**, *165*, 691.
(36) Stumm, W.; Schindler, P. W. In *Aquatic Surface Chemistry*; Stumm, W., Ed.; Wiley: New York, 1987; p 83.
(37) von Zelewski, A.; Bemtgen, J. M. *Inorg. Chem.* **1982**, *21*, 1771.
(38) Parfitt, R. L.; Fraser, A. R.; Russell, J. O.; Farmer, V. C. *J. Soil Sci.* **1977**, *28*, 40.
(39) Kummert, R.; Stumm, W. *J. Colloid Interface Sci.* **1980**, *75*, 373.